

Multimodal Outer Arithmetic Block Dual Fusion of Whole Slide Images and Omics Data for Precision Oncology

Omnia Alwazzan, Amaya Gallagher-Syed, Thomas Millner, Ioannis Patras, *Member, IEEE*, Silvia Marino, Gregory Slabaugh, *Member, IEEE*

Abstract—Developing a central nervous system (CNS) tumor classifier by integrating DNA methylation data with Whole Slide Images (WSI) offers significant potential for enhancing diagnostic precision in neuropathology. Existing approaches typically integrate encoded omic data with histology only once—either at an early or late fusion stage—while reintroducing encoded omic data to create a dual fusion variant remains unexplored. Nevertheless, reintroduction of omic embeddings during early and late fusion enables the capture of complementary information from localized patch-level and holistic slide-level interactions, allowing boosted performance through advanced multimodal integration. To achieve this, we propose a dual fusion framework that integrates omic data at both early and late stages, fully leveraging its diagnostic strength. In the early fusion stage, omic embeddings are projected into a patch-wise latent space, generating omic-WSI embeddings that encapsulate per-patch molecular and morphological insights, effectively incorporating this information into the spatial representation of histology. These embeddings are refined with a multiple instance learning gated attention mechanism to attend to critical patches. In the late fusion stage, we reintroduce the omic data by fusing it with slide-level omic-WSI embeddings using a Multimodal Outer Arithmetic Block (MOAB), which richly intermingles features from both modalities, capturing their global correlations and complementarity. We demonstrate accurate CNS tumor subtyping across 20 fine-grained subtypes and validate our approach on benchmark datasets, achieving improved survival prediction on TCGA-BLCA and competitive performance on TCGA-BRCA compared to state-of-the-art methods. This dual fusion strategy enhances interpretability and classification performance, highlighting its potential for clinical diagnostics.

Index Terms—Multimodal Deep Learning, Dual Fusion, Digital Pathology, Omics, Survival Prediction

I. INTRODUCTION

Manuscript received XXX XX, XXX. The authors appreciate the support of the University of Jeddah and the Saudi Arabia Cultural Bureau. This paper utilised Queen Mary's Andrena HPC facility. This work also acknowledges the support of the National Institute for Health and Care Research Barts Biomedical Research Centre (NIHR203330), a delivery partnership of Barts Health NHS Trust, Queen Mary University of London, St George's University Hospitals NHS Foundation Trust and St George's University of London.

The authors are affiliated with Queen Mary University of London. Corresponding author (e-mail: o.alwazzan@qmul.ac.uk).

DNA methylation is an epigenetic process where methyl groups are added to specific sites on DNA molecules, typically at cytosine bases followed by guanine (CpG sites) [1]. These modifications affect downstream gene expression levels without changing the DNA sequence itself, resulting in heritable changes in gene activity—an effect termed “epigenetic” [2]. Such a process often leads to gene silencing or reduced gene expression by preventing transcription factors from binding to DNA, thereby inhibiting gene activation. In central nervous system (CNS) tumors, DNA methylation patterns offer valuable insights, enabling the differentiation of tumor subtypes, prediction of clinical outcomes, and guidance on treatment strategies [3]—particularly in cases where diagnostics via digitized Whole Slide Images (WSIs) shows high inter-observer variability [4]. Given the aggressive nature of malignant CNS tumors and their associated poor survival rates, there is a critical need to improve diagnostic precision [5]. One study demonstrated altered subtype classifications in 35% of cases, potentially impacting treatment decisions for 4% of pediatric patients [6]. This demand has driven the development of CNS tumor classifiers based on DNA methylation array data, providing significant advancements in neuropathology [4]. The World Health Organization (WHO) has also responded by incorporating molecular profiling alongside traditional histology into the latest CNS tumor classification guidelines, which defines 40 tumor types and subtypes based on key molecular characteristics [7]. Such findings have further inspired research into automated integrative molecular morphology classification systems using artificial intelligence (AI) algorithms, including machine learning (ML) and deep learning (DL), to improve tumor diagnosis and prognosis [4], [8]–[13].

Unimodal Approaches For instance, in the single modality domain, Capper et al. [9] conducted pioneering validation of a methylation-based classification system on 2801 CNS tumor samples using a machine learning (ML) approach [9]. For each CNS tumor subtype included in the classifier, which is referred to as the methylation class, the classifier generated a predicted probability (calibrated score) that summed to 1, with the optimal balance between specificity and sensitivity obtained at 0.84 [14], with tumors with a calibrated score below 0.3 classified as “no match”. Capper’s ML method now serves as an essential aid in the routine diagnostic workup of

CNS tumors [4]. Hwang et al. [15] developed an image-based deep learning model using DNA methylation data to predict the origin of cancer of unknown primary (CUP). By employing a vision transformer algorithm and organ-specific DNA methylation images, their approach shows significant potential for enhancing CUP diagnosis and informing treatment strategies. DNA methylation profiling not only aids in precise classification but also supports surgical strategies specific to CNS tumors, improving surgical outcomes and overall patient care [5]. Djirackor et al. [5] utilize ML algorithms to classify brain tumors in real-time by taking the DNA methylation data of a new tumor sample and comparing it to a database of known methylation signatures, assigning a classification based on the closest match. This allows for fast intraoperative decision-making by providing molecular insights during surgery.

Multimodal Approaches. In the multimodal domain, Hoang et al. [12] developed “Deploy”, a deep learning model designed to predict DNA methylation beta values from histopathologic images. Alternatively, Zheng et al. [16] demonstrated that classical machine learning algorithms can link DNA methylation profiles of cancer samples with morphometric features from whole slide images (WSIs), showing improved model performance when genes are grouped into methylation clusters. Interestingly, Sturm et al. [17] explores the use of a multiomic approach — integrating data such as genomics, transcriptomics, and epigenomics — to improve the diagnostic accuracy of pediatric brain tumors, which are often challenging to classify due to overlapping histological features. This method enhances diagnostic precision, allowing for better treatment decisions in pediatric neuro-oncology. However, few studies [12] have combined epigenetic data with WSIs, primarily due to both modalities’ significant data size and complexity, which require extensive preprocessing and advanced fusion techniques to address their heterogeneity. In contrast, multimodal DL approaches combining histology and omic data for improved survival prediction have gained considerable attention in recent years [8], [10], [11], [13], [18]–[25]. In particular, several studies [10], [13], [22], [26] have highlighted the value of different fusion stages (early or late), particularly emphasizing early fusion for its ability to create an explainable framework from heterogeneous data. However, Zhang et al. [20] argue that early or late fusion methods can partially overlook modality-specific information, potentially leading to a decline in quantitative or qualitative performance. Accordingly, they propose a prototypical information bottleneck to maintain modality-specific information while simultaneously reduce redundancy. Furthermore, a joint distribution of feature embeddings is used to maintain mutual information between omic and WSI modalities. Despite the promising performance of multimodal approaches in medical diagnostics, significant challenges remain in effectively integrating and analyzing diverse data types, particularly in the context of CNS tumor subtyping. Our critical assessment of existing methods reveals three key gaps:

1) *Limitations of WSI*: While WSI serves as a primary diagnostic tool for pathologists, accurately identifying fine-grained tumor subtypes based on morphology alone is challenging due to visual feature overlap among CNS subtypes. This similarity

risks including irrelevant tumor regions and highlights the need for complementary data sources to achieve more precise subtyping [4]

2) *Constraints of DNA methylation classification*: DNA methylation classifiers have demonstrated high accuracy in tumor subtyping, but they lack the ability to connect this accuracy to specific regions within WSIs. The main limitation is that these classifiers focus solely on DNA methylation profiles without considering the spatial context provided by WSIs. This constraint limits their capacity to capture how epigenetic patterns contribute to the morphological characteristics observed in specific regions, ultimately reducing the interpretability and comprehensive understanding that could be achieved through integration with WSI data.

3) *Scarcity of integrative models for CNS tumor subtyping*: This challenge is particularly acute in the context of central nervous system tumors, where the inherent heterogeneity and massive size of both DNA methylation arrays (typically 850k one-dimensional vectors) and WSIs (represented with large, multi-dimensional matrices) have received limited attention. The lack of effective multimodal fusion methods in this domain presents an opportunity to leverage the powerful discriminative capacity of DNA methylation data to improve subtyping and enhance the clinical translation of these advanced imaging and molecular techniques. Addressing these gaps requires innovative approaches to data fusion, potentially exploring both early and late fusion strategies, to fully leverage the complementary strengths of WSI and DNA methylation data in CNS tumor subtyping.

A. Contributions

Answering these challenges, we propose a novel dual fusion approach to improve CNS tumor subtyping by integrating DNA methylation data with WSIs. We design MOAD-Net, a **Multimodal Outer Arithmetic Dual Fusion Network** that combines two fusion variants: early fusion focused on capturing essential local interactions and late fusion for broader, richer cross-modal correlations, ultimately providing complementary insights and improving the model’s decision-making process. This dual fusion strategy provides a comprehensive, holistic integration of cross-modal data, maximizing the strengths of each fusion type. We summarize the significance of each of our contributions:

- **Importance of early fusion**: The early fusion stage enriches interpretability by embedding DNA data directly into each WSI patch, allowing the model to capture detailed, localized interactions. This granularity is essential for identifying unique features within tumor subtypes, especially in cases where subtle variations are critical for accurate subtyping.
- **Significance of late fusion**: In contrast, late fusion stage leverages global slide-level associations, capturing high-level, complementary relationships between WSI and omic data.
- **Effectiveness and state-of-the-art results**: This combined approach makes MOAD-Net the first method to leverage the BRAIN UK dataset in an imaging-omics

pipeline, achieving exceptional results by accurately distinguishing complex brain tumor subtypes. Extensive ablation studies on the TCGA benchmark datasets further validate MOAD-Net’s performance. Our method achieves SOTA survival prediction on the BLCA dataset and competitive results on the BRCA dataset, underscoring its effectiveness across diverse multimodal applications.

We argue that using a late fusion variant alone would capture only global interactions between the WSI level label and epigenetic data, lacking the interpretability needed for accurate subtyping [13], [27]. On the other hand, an early fusion approach alone would focus exclusively on local interactions, neglecting the broader relationships between modalities [27], which we confirmed empirically with extensive experiments. Our proposed dual fusion framework, MOAD-Net, addresses these limitations by combining early and late fusion strategies, creating a new variant that uniquely captures both local and global interactions across modalities and enhances interpretability and overall classification accuracy.

Note that, this paper extends our previous conference paper [28] by implementing a dual fusion architecture, working with three additional imaging-omics datasets, recently proposed SOTA backbones, and shows how heatmaps can be generated, providing interpretability.

II. STUDY DESIGN

A. Datasets

The following sections briefly provide an overview of the datasets used to evaluate MOAD-Net.

1) *Slide Subtyping: UK BRAIN Brain Tumor Dataset* [29]: We obtained WSIs and matched DNA methylation data from the UK Brain Archive Information Network (BRAIN UK)¹. The dataset includes (H&E)-stained WSIs from 1,504 patients, covering 20 subtypes, primarily glioblastoma and other glial tumors (left upper corner of Fig. 4). This data exhibits significant class imbalance across its 20 subtypes, with some classes heavily underrepresented, as shown in Fig. 2. To address this, we perform 2-fold cross-validation to ensure all slides in the dataset are covered, and we report the average performance across the two folds for all metrics. For WSIs, we used QuPath² for tissue segmentation and tiling, generating 1M patches (4K–10K per slide). For the tissue methylation profile, We processed raw idat files to extract DNA methylation CpG sites using the hg38 Illumina array with EPICv1 annotation, following the workflow in [30]. We calculated m-Values to quantify methylation levels, producing a matrix of 850k CpG sites for 1,504 patients. To reduce features, we applied variance, coefficient of variation (CV), median absolute deviation, and interquartile range, selecting the 8K most variable CpG sites by intersecting these methods. We experimented with clustering 4K CpG sites and Random Forest selection of 10K sites, as suggested in the literature, but 4K reduced performance and 10K showed no improvement, leading us to select 8K CpG sites.

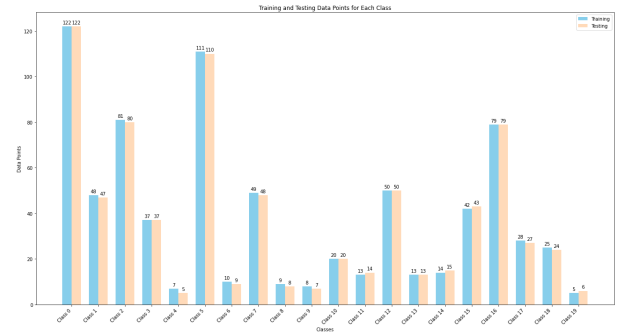


Fig. 2. Distribution of training and testing data points across 20 classes/subtypes. The bar chart illustrates the number of patients allocated to training and testing sets for each class, highlighting the balance of data used for model development and evaluation.

2) *Survival prediction: TCGA Datasets*: To showcase MOAD-Net’s versatility and compare it with other omic-WSI fusion methods [8], [10], [13], [22], [31], we evaluate its performance on The Cancer Genome Atlas (TCGA) datasets for Bladder Urothelial Carcinoma (BLCA) ($n = 359$) and Breast Invasive Carcinoma (BRCA) ($n = 869$), using the survival prediction task outlined by Jaume *et al.* [13]. We utilized a coupled set of 331 biological pathways derived from 4,999 distinct genes. These genes were grouped into pathways based on their functional interactions and roles in biological processes relevant to the BLCA and BRCA datasets.

B. Multimodal Outer Arithmetic Dual Fusion Network (MOAD-Net)

We designed a multimodal fusion framework, shown in Fig. 1, that integrates omic data and WSIs through both early and late fusion stages. Our proposed method, MOAD-Net, is aimed at multimodal brain tumor subtyping, and survival prediction in both lung and breast cancer. In the following subsection, we highlight key components of the MOAD-Net framework.

1) *Omic Encoder*: To construct the omic encoder, we followed the established practice of using a Self-Normalizing Neural (SNN) [32] consisting of two fully connected layers, where each layer applies an Exponential Linear Unit (ELU) activation function followed by Alpha Dropout (0.25) that compress the 8K CpG sites into an encoded omic feature $\mathbf{o}_i \in \mathbb{R}^{d^o}$ $d^o = 256$. Note that for comparison studies [13], [18], [20], [22], we used the same encoder tokenizing the genes into a group of pathways to draw a fair comparison.

2) *Whole Slide Image Encoder*: For a WSI \mathbf{X} , we extract a collection of patches, represented as $\mathbf{x}_{i0}, \mathbf{x}_{i1}, \dots, \mathbf{x}_{ij}$; where i denotes the patch index and j indicates the variable number of patches across different slides. We extract non-overlapping patches from tissue areas at a 20 \times magnification (about 0.5 $\mu\text{m}/\text{pixel}$ resolution). Subsequently, we utilized a SOTA vision-only encoder [11] UNI to obtain the patch embeddings \mathbf{e}_{ij} . Using UNI $f_{enc}(\cdot)$, we derive a set of low-dimensional patch embeddings for each patient, where $\mathbf{e}_{ij} = f_{enc}(\mathbf{x}_{ij}) \in \mathbb{R}^{d^e}$, $d^e = 1024$, serving as input to our pipeline.

3) *Fusion Stages*: The fusion scheme is the key contribution of this work. Our motivation sparks from the enhanced features

¹<https://www.southampton.ac.uk/brainuk/>

²<https://qupath.github.io/>

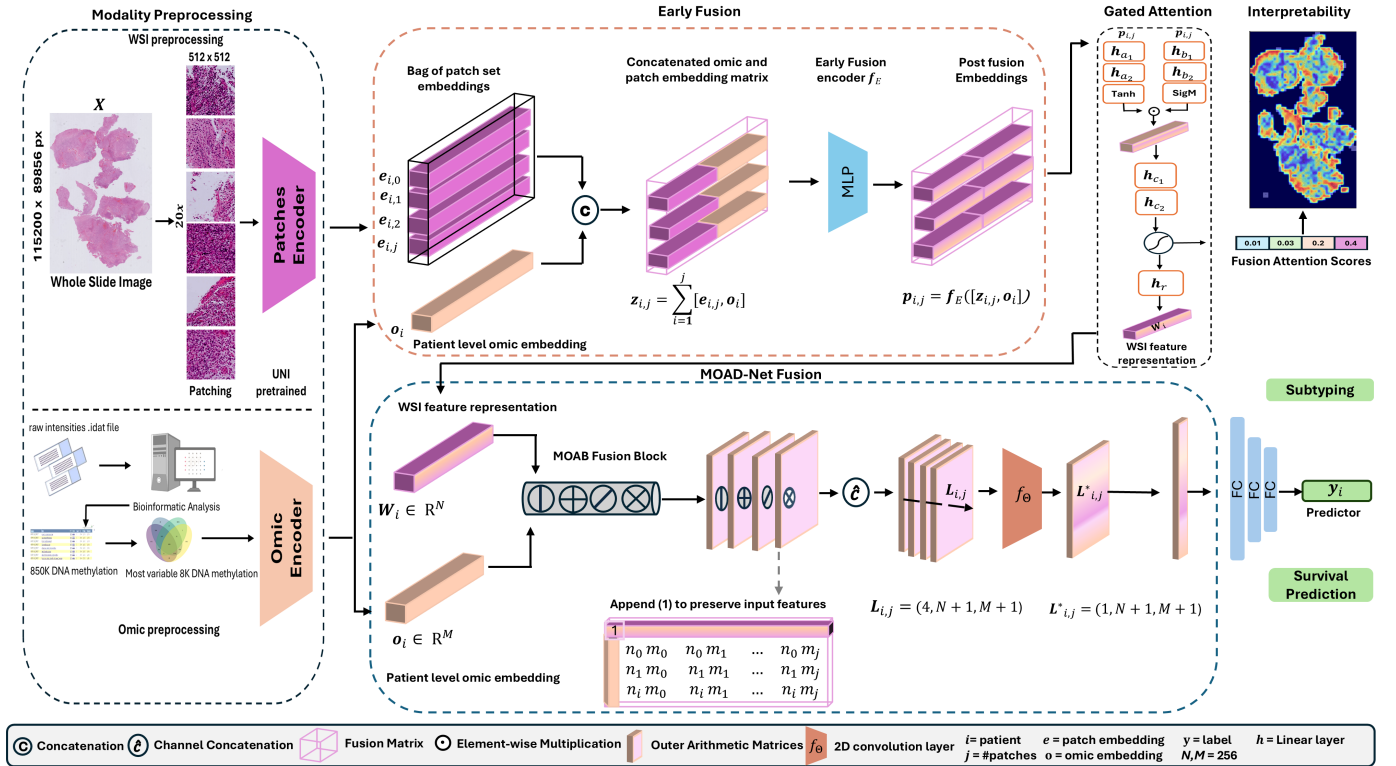


Fig. 1. An overview of the proposed MOAD-Net framework. Data engineering and encoding for each modality are performed in the preprocessing block. The early fusion block (top) then receives encoded inputs from both modalities, where omic data is concatenated to form a matrix $z_{i,j}$ which is processed by an MLP encoder that learns a joint mapping, resulting in output $p_{i,j}$. A gated, weighted MIL score is then estimated to indicate patch importance providing heatmap interpretability and producing a WSI feature W_i . Next, the MOAD-Net fusion block (bottom) reintroduces omic features o_i alongside the W_i slide-level feature from the early fusion block as input to the MOAB fusion block. This block performs four outer arithmetic operations to create fusion representations, which are further reduced with f_θ before being sent to the final subtyping classifier.

obtained from the dense modeling conducted by multimodal early fusion methods in [10], [13], [22], [26]. Hence, we divide this subsection into two: *early fusion* and *late fusion*.

Early Fusion, given a matrix of patch embeddings e_{ij} and the DNA feature vector o_i for patient i , the encoded omic feature vector is cloned to match the number of patches in the WSI. This results in a tensor of shape (N_i, d_o) , where N_i is the number of patches in WSI i , and d_o is the dimension of the DNA feature. The combined feature set for patient i is represented as:

$$\mathbf{z}_{ij} = [e_{ij}, \mathbf{o}_i] \quad (1)$$

Here, $\mathbf{z}_{ij} \in \mathbb{R}^{d_e+d_o}$ represents the concatenated $[\cdot]$ feature vector for patch j in WSI i , and the resulting shape becomes $(N_i, d_e + d_o)$. Next, a Multilayer Perceptron (MLP) encoder, denoted as f_E , is applied to each concatenated patch embedding and omic feature pair to learn their joint representation:

$$\mathbf{p}_{ij} = f_E([\mathbf{z}_{ij}, \mathbf{o}_i]) \quad (2)$$

This operation is performed for all patches j of the i th patient. By incorporating omic features o_i into patch embeddings via early fusion, we enrich the representation with complementary molecular information. Leveraging an Attention-based Deep Multiple Instance Learning (ABMIL) approach [33], we capture patch-level discriminative features that synergistically combine molecular and morphological insights,

enabling more precise identification of critical regions. The resulting embedding is projected to a slide-level representation $W_i \in \mathbb{R}^{256}$, dimensionally aligned with the original omic feature o_i to facilitate subsequent late fusion.

Late Fusion, motivated by [13] in modeling the interaction between omic to histology, histology to omic, and omic to omic, we mimic a similar behavior by employing, for the first time in journal form, a novel multimodal outer arithmetic fusion block (MOAB) [28] within a dual fusion approach, marking a new direction in combining MOAB with dual fusion to enhance modality integration. MOAB inputs (W_i, o_i) will be fused through four operations: outer product, outer division, outer subtraction, and outer addition. MOAB extracts various interactions while simultaneously preserving the W_i input feature by appending one to each input embedding when performing the outer product and division fusion and zero in the case of the outer subtraction and addition fusion. To simplify this, given the two embeddings W_i, o_i $W_i \in \mathbb{R}^{N \times 1}$ and $o_i \in \mathbb{R}^{M \times 1}$. Initially, we append a 1 to each embedding, i.e., $W_{i1} = [1; W_i]$ and $o_{j1} = [1; o_j]$. Their outer product is defined as

$$(W_{i1} \otimes o_{j1})_{ij} = W_{i1} * o_{j1}, \quad (3)$$

for $i \in [1 \dots N + 1]$ and $j \in [1 \dots M + 1]$ yielding a $(N + 1) \times (M + 1)$ matrix that intermingles every element of W_{i1} with every element of o_{j1} . The appended 1 in both W_{i1} and o_{j1} ensures the original unimodal features W_i and o_j appear in

the outer product matrix. Similarly, we define outer division, addition, and subtraction as

$$(\mathbf{W}_{i0} \oplus \mathbf{o}_{j0})_{ij} = \mathbf{W}_{0i} + \mathbf{o}_{0j} \quad (4)$$

$$(\mathbf{W}_{i0} \ominus \mathbf{o}_{j0})_{ij} = \mathbf{W}_{0i} - \mathbf{o}_{0j} \quad (5)$$

$$(\mathbf{W}_{i1} \oslash \mathbf{o}_{j1})_{ij} = \mathbf{W}_{1i} \div (\mathbf{o}_{1j} + \epsilon) \quad (6)$$

where ϵ is a small number, and $\mathbf{W}_{i0} = [0; \mathbf{W}_i]$ and $\mathbf{o}_{j0} = [0; \mathbf{o}_j]$.

The four matrices produced by MOAB are concatenated along the channel dimension to form a multimodal tensor $\mathbf{L}_{ij} \in \mathbb{R}^{4 \times 257 \times 257}$. We hypothesize that channel fusion will maintain the proximity of closer points and will use fewer parameters compared to a typical concatenation. By combining features across the channel dimension, we greatly decrease the dimension of the following fully connected layer from $(257 \times 257)^4$ to $(257)^2$. Following the same parameters in [28], a 2D convolution layer is subsequently performed to leverage associated interactions, resulting in a singular condensed multimodal feature tensor $L_{ij}^* \in \mathbb{R}^{1 \times 257 \times 257}$. Last, we flatten \mathbf{L}_{ij}^* and apply leaky ReLU followed by a linear predictor for brain tumor subtyping prediction. We hypothesize that MOAB simple yet effective operations adapt similar interactions conducted in [13] and rather excel fusion methods in [13] without introducing any approximation method.

4) *Interpretability*: Employing ABMIL on the post-fusion embedding, \mathbf{p}_{ij} enables the visualization of attention scores, which provide an enriched perspective on the tumor's phenotype and genotype. This, in turn, enhances ABMIL's capacity to prioritize patches that are biologically relevant. Inspired by [13], we define our gated attention computation as follows:

$$\begin{aligned} \mathbf{h}_{ij} &= \tanh(\mathbf{W}_p \mathbf{p}_{i,j} + \mathbf{b}_p) \odot \sigma(\mathbf{W}_g \mathbf{p}_{i,j} + \mathbf{b}_g), \\ \mathbf{a}_{ij} &= \frac{\exp(\mathbf{w}^T \mathbf{h}_{ij})}{\sum_1^j \exp(\mathbf{w}^T \mathbf{h}_{ij})}, \\ \mathbf{W}_i &= f_\rho \left(\sum_{j=1}^j \mathbf{a}_{ij} \mathbf{h}_{ij} \right), \end{aligned} \quad (7)$$

Here, \mathbf{W}_p and \mathbf{W}_g are learnable parameters for the input and gating functions, respectively, with \mathbf{b}_p and \mathbf{b}_g as their corresponding biases. The symbol \odot denotes element-wise multiplication, and σ represents the sigmoid activation function. The gated embedding for patch j in sample i is given by \mathbf{h}_{ij} , while \mathbf{a}_{ij} represents the attention weight for patch j , normalized across all patches. We leverage \mathbf{a}_{ij} at inference to generate the heatmap shown in Fig. 5. To further enhance our late fusion stage, we weight \mathbf{W}_i with \mathbf{a}_{ij} using an MLP f_ρ which consists of a linear transformation, an activation function (ReLU), and dropout. f_ρ is applied to the pooled embedding \mathbf{W}_i increases its representational power, making it a more refined input for the late fusion stage. This enriched embedding encapsulates a high-level representation of the WSI, effectively integrating morphological and molecular insights from the attention mechanism.

III. EXPERIMENTS

A. Performance Metrics

For the subtyping task, we assessed performance utilizing various metrics: F1-Macro, F1-Micro, Precision, and Recall/Sensitivity. F1-Macro is a significant metric for our quantitative analysis as it independently computes the F1 score for each class and subsequently averages them, assigning equal weight to each class irrespective of its size, thereby ensuring that the performance of minority classes is not overwhelmed by that of majority classes. For the survival prediction task, we chose performance metrics comparable to related work. Following an identical implementation to [13], [20], [22], For the survival prediction task, we define survival analysis as estimating the probability of an event occurring within a given survival time, while accounting for right-censored data. Censorship status is represented as $c \in \{0, 1\}$, where $c = 0$ denotes an observed event (e.g., death) and $c = 1$ indicates the patient's last known follow-up. Following previous work [13], [20], [22], we discretize the time-to-event into non-overlapping time intervals $(t_{i-1}, t_i]$, based on the quartiles of survival times, and denote it as y_i . This formulation transforms the problem into a classification task with censorship information, where each patient is represented by $(\mathbf{L}_{\text{logits}}, y_i, c)$.

Next, we use the dual fusion embedding generated by MOAB, $\mathbf{L}_{\text{logits}}$, to predict the discretized bin corresponding to a time interval t_i . We define the discrete hazard function as:

$$f_{\text{hazard}}(y_i | \mathbf{L}_{\text{logits}}) = \sigma(y_i),$$

where σ is the sigmoid activation function. Intuitively, $f_{\text{hazard}}(y_i | \mathbf{L}_{\text{logits}})$ represents the probability that the patient experiences the event (e.g., death) during the interval $(t_{i-1}, t_i]$.

The discrete survival function is then defined as:

$$f_{\text{surv}}(y_i | \mathbf{L}_{\text{logits}}) = \prod_{k=1}^{i-1} (1 - f_{\text{hazard}}(y_k | \mathbf{L}_{\text{logits}})),$$

which represents the probability that the patient survives up to the interval $(t_{i-1}, t_i]$.

The Negative Log-Likelihood (NLL) survival loss is formally defined as:

$$\begin{aligned} \mathcal{L} \left(\{\mathbf{L}_{\text{logits}}, y, c\}_{i=1}^{N_{\text{total}}} \right) &= - \sum_{i=1}^{N_{\text{total}}} \left[c_i \log (f_{\text{surv}}(y_i | \mathbf{L}_{\text{logits}})) \right. \\ &\quad \left. + (1 - c_i) \log (f_{\text{surv}}(y_i | \mathbf{L}_{\text{logits}}) - 1[y_i]) \right. \\ &\quad \left. + (1 - c_i) \log (f_{\text{hazard}}(y_i | \mathbf{L}_{\text{logits}})) \right]. \end{aligned} \quad (8)$$

where (N_{total}) is the total number of samples in the dataset, and (k) corresponds to the total number of discretized labels. As noted in [13], this approach enhances survival analysis by accurately estimating survival probabilities, predicting event timestamps, and rigorously accounting for censorship status.

Note that in the ACMIL model proposed by Zhang et al. [23], the authors employed a composite loss function that integrates cross-entropy loss with a diversity loss designed to enhance the variability of the attention distribution across various regions of the WSI image. To modify ACMIL for survival analysis, we integrated the NLL loss with the diversity loss to emulate the learning methodology employed in the original study [23].

B. Domain Specific Prior Work and Ablation Studies

To evaluate our method on subtyping and survival prediction tasks, we replicate and adapt recent SOTA methods by incorporating MOAB as a replacement for the fusion technique initially used in these methods. For the survival prediction task, we conducted a comparative analysis using a consistent feature extractor across all modalities, including WSI and omic data, utilising the recent TCGA ID samples from [13]. We uniformly implemented training hyperparameters and loss functions across all models displayed in Tables I and III. To this end, this section is divided into two parts. SOTA baseline models detailing unimodal and fusion models employed for each task, together with ablation studies included in Tables I, III, and IV.

1) *State-of-the-Art Baseline Models*: We evaluate our approach against SOTA techniques in the: 1) *Unimodal* and 2) *Multimodal setting* for both tasks, subtyping and survival prediction.

For the **subtyping** task:

- *Unimodal techniques*, we utilize MLP and SNN [32] as baseline models for the DNA methylation data. For WSI, we utilize Attention-based Multiple Instance Learning (ABMIL) [18], which implements gated weighted attention pooling to determine the importance of patches, and Transformer-based Multiple Instance Learning (TransMil) [31], which employs self-attention mechanisms from Transformers to evaluate correlations among patches in WSI. Through rigorous experimentation, we found that ABMIL outperforms the TransMIL baseline in both performance and computational efficiency, making it the preferred baseline for MOAD-Net, as also noted in [34].
- *Multimodal techniques*, we adapt Attention Challenging Multiple Instance Learning (ACMIL) [23] to work in a multimodal setting. ACMIL [23] is an approach proposed by Zhang et al. to address overfitting issues in MIL for single modality WSI classification. It employs multiple attention branches to identify varied discriminative patterns among instances, thereby distributing attention across the WSI and avoiding excessive concentration on a limited set of critical patches. Furthermore, TransMIL [31], with two late fusion variants, concatenation (Cat) and Kronecker product (KP), was conducted. We also utilize MCAT [10] and SurvPath [13], both of which perform multimodal tokenization to extract histology and biological pathway tokens. These tokens are then processed through a co-attention Transformer to model interactions between the different modalities. MCAT and SurvPath represent transformer-based early fusion approaches that integrate multimodal features at an initial stage. To maintain architectural consistency, we opted not to replace concatenation with the MOAB late fusion block in these models. The complex architectures of MCAT and SurvPath could be destabilized by MOAB, potentially introducing noise without improving performance. However, to test our dual fusion hypothesis, we replicated these models with a \mathbf{p}_{ij} early fusion input representation, enabling each model to leverage two distinct

fusion stages. By comparing the performance of SurvPath and MCAT with \mathbf{p}_{ij} to their single-stage counterparts (SurvPath* and MCAT*), we provide empirical evidence that dual fusion outperforms single-stage fusion methods.

For the **survival prediction** task:

- *Unimodal techniques*, in addition to aforementioned unimodal models implemented for subtyping, we employed Spars-MLP [13], which tokenized transcriptomics into biological pathway tokens that encode specific cellular functions for the downstream analysis.
- *Multimodal techniques*, we integrated MOAD-Net across the same models used in subtyping tasks excluding MCAT, and including prototypical information bottlenecking and disentangling (PIBD) [20] method. PIBD [20] uses a prototypical information bottleneck to compress and align representations from different modalities, reducing complementary information redundancy while keeping the expressiveness of modality-specific information. It also introduces a disentanglement mechanism to separate modality-specific (WSI, omic) and shared information to integrate multimodal data. For PIBD experiments, we restricted MOAB to a late fusion setting, respecting PIBD's initial modality-specific separation. Introducing MOAD-Net in an early fusion setting could potentially conflict with this initial modality independence, underscoring our strategic late fusion choice to maintain alignment with PIBD's architectural principles.

2) *Ablation studies*: For the subtyping task, the core focus of our work is the dual fusion approach. We conducted ablation studies using only MOAD-Net within the Dual Fusion framework, while all other results detailed in Table I that are without MOAD-Net indicators showed late fusion outcomes. Moreover, for a comprehensive evaluation of MOAD-Net, we conducted three ablation experiments (detailed in Table II); In the first experiment, we removed the MOAB fusion block, using only ABMIL. Here, \mathbf{p}_{ij} served as the input to ABMIL, and the resulting feature embedding \mathbf{W}_i was directly fed to the classifier layer to assess the distinct impact of both ABMIL and the DNA modality. In the second experiment, we removed the early fusion block (illustrated in Fig. 1), making \mathbf{e}_{ij} the input to the gated attention block, which is then followed by the MOAD-Net fusion block. The results indicate a reasonable overall accuracy, reflecting the complexity of subtype classification; however, they also underscore the need for advanced fusion techniques to leverage complementary features across modalities effectively. Last, we employed a task-agnostic encoder, ConvNext.v2 [35], pre-trained on ImageNet, to extract features from the WSI and tested MOAD-Net with this setup. We also explored an alternative configuration, placing the MOAB fusion block in the early fusion stage, which revealed two primary issues. First, element-wise multiplication in each outer arithmetic operation required reducing both feature dimensions to less than 64 to manage the high patch count (up to 10K per WSI), resulting in substantial information loss and suboptimal performance. Second, this approach demanded computational power and memory resources that exceeded feasible limits due to the large

number of patches.

For the survival prediction task, we extensively evaluated the MOAD-Net approach using the two most common baseline fusion models: ABMIL [33] and TransMIL [31]. We adopted two late fusion techniques: concatenation (Cat) and Kronecker product (KP). These were compared with MOAD-Net within both fusion settings, as shown in Table IV.

C. Data and Code Availability

For brain tumor subtyping, we obtained data from BRAIN UK through a rigorous application process, securing anonymized tissue samples and epigenetic data from NHS Neuropathology Centers. For survival prediction, WSIs are publicly available through the TCGA repository, with corresponding omic data accessible from ³. Source code will be made available upon acceptance.

IV. RESULTS

A. Subtyping and survival prediction

Quantitative subtyping and survival prediction results are depicted in Tables I and III. Overall, MOAD-Net integrated with ABMIL consistently demonstrates superior performance in brain tumor subtyping and BLCA survival prediction, and achieves competitive performance with the best models for BRCA across recent methodologies [13], [19], [20], [23]. For the subtyping task, Table I shows that the SNN model performs well across metrics when using omics-only data, closely followed by the MLP model with slightly lower scores. These results indicate that omics data alone offers strong predictive power, though further improvements and interpretability may be limited without incorporating WSI data. Conversely, WSI only models exhibit relatively low performance across metrics, likely due to indistinguishable patterns among most subtypes and the presence of rare classes represented by only a few large slides, making it challenging to obtain sufficient information for high accuracy. These limitations emphasize the importance of multimodal fusion for enhancing interpretability and performance. In a multimodal setting, ABMIL-MOAD-Net achieves the best scores across all metrics, establishing it as the top performing model in the subtyping task and demonstrating the MOAD-Net architecture’s effectiveness in leveraging multimodal data to provide a richer, more informative representation. Notably, integrating MOAD-Net with advanced architectures like TransMIL and ACMIL significantly improves performance (F1-Micro and Recall) compared to using these models without MOAD-Net. Qualitative results in Fig. 4 further illustrate MOAD-Net’s effectiveness in classifying most tumor subtypes, showcasing the strong impact of its intermingled features. To assess class separation accuracy in the t-SNE representations, we calculated silhouette scores for early and late fusion t-SNE plots, as they displayed visually similar patterns. The late fusion t-SNE achieved a silhouette score of 0.33, while MOAD-Net scored 0.37, indicating that MOAD-Net provides more accurate class

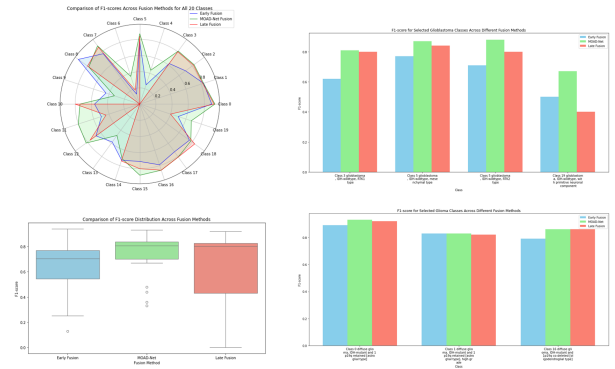


Fig. 3. Comparison of F1-scores across different fusion methods for glioma classification. The radar chart illustrates the F1-score performance across all 20 classes, highlighting distinct patterns for Early Fusion, MOAD-Net, and Late Fusion. The bar plots zoom in on specific glioblastoma and glioma classes, showing class-level performance variations across fusion methods. The box plot provides a summary of F1-score distributions, showcasing the variability and consistency of each fusion method.

separation. This is also evident in the box plot in Fig. 3, where MOAD-Net displays fewer low outliers and a more compact distribution than early and late fusion.

The confusion matrices demonstrate that the early fusion method significantly boosted MOAD-Net’s accuracy in classifying subtypes, especially for minority classes. Notably, classes 6, 9, and 13, which went unclassified with the late fusion method, were correctly identified with early fusion and MOAD-Net, with our method achieving the best performance overall. Conversely, late fusion performed better in classes 2 and 16, highlighting the challenges of handling heterogeneous multimodal data that can lead to misclassification in MOAD-Net. This also underscores the need for tailored fusion techniques to address different data complexities. The clear diagonal in the confusion matrix across all fusion methods confirms the effectiveness of using both early and late fusion techniques within MOAD-Net’s dual fusion framework, emphasizing the distinct contributions of each fusion approach in various scenarios. Furthermore, Fig. 3 illustrates that MOAD-Net’s dual fusion approach significantly enhanced classification of all glioblastoma subtypes (4 groups) and diffuse glioma subtypes (4 groups), even in cases with highly overlapping morphological features.

For the survival prediction task, integrating MOAD-Net with existing (SOTA) models (indicated by *) demonstrates a constant performance improvement over their standalone counterparts, emphasizing the value of MOAD-Net’s rich intermingled features. These features enhance the c-index scores across multiple methods, making MOAD-Net particularly effective in predicting patient disease-specific survival for BLCA, where it outperforms all other methods and achieves competitive results in BRCA. Prototype-based methods, such as PIBD and MMP, show notable performance gains on BRCA data compared to other approaches. To further explore this, we integrated MOAB within PIBD [20], achieving results comparable to the leading model [22]. However, we did not test MOAB with MMP [27] because MMP already incorporates two early fusion stages (transformer and optimal transport). Adding MOAB would

³https://github.com/mahmoodlab/SurvPath/tree/main/datasets_csv/metadata

TABLE I

SUBTYPING PREDICTION MOAD-NET RESULTS ON THE UK BRAIN DATASET. WE SHOW MOAD-NET COMBINED WITH SOTA BASELINE MODELS. THE BEST PERFORMANCE IS HIGHLIGHTED IN **BOLD. CONCATENATION AND KRONECKER PRODUCTS ARE DENOTED BY (CAT) AND (KP). THE DARKER GRAY ROWS REPRESENT MODELS ENHANCED BY INTEGRATING MOAD-NET OR USING ITS EARLY FUSION EMBEDDINGS p_{ij} , DEMONSTRATING IMPROVED PERFORMANCE COMPARED TO STANDALONE BASELINE MODELS.**

Model	F1-Ma	F1-Mi	Prec	Recall
Omics				
SNN	0.726 ± 0.003	0.819 ± 0.013	0.799 ± 0.015	0.715 ± 0.023
MLP	0.69 ± 0.012	0.794 ± 0.021	0.741 ± 0.018	0.684 ± 0.031
WSI				
ABMIL	0.247 ± 0.004	0.442 ± 0.004	0.280 ± 0.224	0.256 ± 0.250
TransMIL	0.217 ± 0.019	0.434 ± 0.003	0.240 ± 0.024	0.230 ± 0.013
Multimodal				
ACMIL MOAD-Net	0.501 ± 0.011	0.729 ± 0.031	0.602 ± 0.032	0.490 ± 0.014
TransMIL (Cat)	0.711 ± 0.005	0.799 ± 0.005	0.744 ± 0.003	0.707 ± 0.002
TransMIL (KP)	0.483 ± 0.003	0.741 ± 0.016	0.485 ± 0.007	0.506 ± 0.008
TransMIL MOAD-Net	0.724 ± 0.005	0.816 ± 0.002	0.759 ± 0.009	0.719 ± 0.001
MCAT	0.402 ± 0.046	0.661 ± 0.021	0.408 ± 0.045	0.414 ± 0.039
MCAT p_{ij}	0.432 ± 0.015	0.703 ± 0.017	0.441 ± 0.031	0.446 ± 0.011
SURVPATH	0.424 ± 0.008	0.697 ± 0.012	0.478 ± 0.038	0.425 ± 0.013
SURVPATH p_{ij}	0.531 ± 0.008	0.761 ± 0.008	0.632 ± 0.005	0.520 ± 0.007
ABMIL (Cat)	0.718 ± 0.013	0.806 ± 0.002	0.764 ± 0.018	0.717 ± 0.023
ABMIL (KP)	0.447 ± 0.024	0.737 ± 0.020	0.481 ± 0.043	0.464 ± 0.032
ABMIL MOAD-Net	0.745 ± 0.025	0.820 ± 0.013	0.769 ± 0.016	0.745 ± 0.035

TABLE II

SUBTYPING PREDICTION ABLATION STUDY OF MOAD-NET SHOWING THE PERFORMANCE OF EARLY, LATE, AND DUAL FUSION METHODS.

Ablation	Model Description	F1-Ma
ABMIL	Early fusion with p_{ij}	0.644 \pm 0.010(−0.10)
ABMIL - MOAB	Late fusion with e_{ij}	0.690 \pm 0.030(−0.05)
MOAD-Net	ConvNeXt encoder	0.732 \pm 0.012(−0.01)
MOAD-Net	Full model	0.745 \pm 0.035

bring the total to four fusion stages, potentially introducing additional complexity and noise without clear performance benefits. While our method demonstrates promising performance across multiple tasks, it's essential to acknowledge some limitations. MOAD-Net faces three primary challenges: first, with dual fusion stages, controlling redundant features from omic data becomes limited. These redundancies can potentially hinder the model's ability to accurately predict certain subtypes, as seen in the confusion matrix where classes 2 and 3 in MOAD-Net score lower than the ablated models shown in Fig. 4B and C. Second, balancing early and late fusion presents a trade-off; although MOAD-Net leverages both stages to capture the strengths of each, finding the optimal balance

TABLE III

SURVIVAL PREDICTION RESULTS OF MOAD-NET WITH BASELINES FOR PREDICTING PATIENT DISEASE-SPECIFIC SURVIVAL USING THE C-INDEX. THE BEST PERFORMANCE IS HIGHLIGHTED IN **BOLD, AND THE SECOND-BEST PERFORMANCE IS UNDERLINED. OVER FIVE RUNS, THE STANDARD DEVIATION IS REPORTED IN BRACKETS. METHODS MARKED * ARE RE-IMPLEMENTED.**

Model	BLCA (\uparrow)	BRCA (\uparrow)
WSI		
ABMIL* [33]	0.572 \pm 0.084	0.573 \pm 0.097
TransMIL* [31]	0.579 \pm 0.052	0.611 \pm 0.119
Omics		
MLP*	0.660 \pm 0.060	0.569 \pm 0.084
SNN*	0.671 \pm 0.058	0.574 \pm 0.112
S-MLP*	0.658 \pm 0.053	0.598 \pm 0.104
Multimodal		
PIBD [20]	0.667 \pm 0.061	0.736 \pm 0.072
PIBD* - MOAB	0.684 \pm 0.046	<u>0.749</u> \pm 0.062
MMP [22]	0.628 \pm 0.064	0.753 \pm 0.096
MMP [22]	0.635 \pm 0.064	0.738 \pm 0.096
ACMIL* - MOAD-Net [23]	0.658 \pm 0.068	0.661 \pm 0.082
TransMIL* - MOAD-Net	0.661 \pm 0.053	0.675 \pm 0.068
SurvPath [13]	0.625 \pm 0.056	0.655 \pm 0.089
SurvPath* - p_{ij}	0.660 \pm 0.047	0.665 \pm 0.006
MBFusion [19]	---	0.644 \pm 0.020
ED-GNN [24]	---	0.672 \pm 0.059
MoME [36]	<u>0.686</u> \pm 0.041	---
MuGI [37]	0.681 \pm 0.056	---
ABMIL MOAD-Net(Ours)	0.691 \pm 0.069	0.726 \pm 0.049

TABLE IV

SURVIVAL PREDICTION. COMPARISON OF C-INDEX FOR BRCA AND BLCA DATASETS USING ABMIL AND TRANSMIL MODELS WITH TWO FUSION STAGES, LATE (LF) AND DUAL (DF), ACROSS THREE AGGREGATION METHODS

BRCA (\uparrow)				
Model	Fus-S	Cat	KP	MOAB
TransMIL	LF	0.606 \pm 0.064	0.602 \pm 0.089	0.620 \pm 0.115
	DF	0.623 \pm 0.032	0.645 \pm 0.067	0.675 \pm 0.068
ABMIL	LF	0.625 \pm 0.075	0.616 \pm 0.090	0.711 \pm 0.095
	DF	0.634 \pm 0.023	0.640 \pm 0.058	0.726 \pm 0.049
BLCA (\uparrow)				
Model	Fus-S	Cat	KP	MOAB
TransMIL	LF	0.599 \pm 0.081	0.582 \pm 0.053	0.600 \pm 0.108
	DF	0.624 \pm 0.068	0.595 \pm 0.052	0.661 \pm 0.053
ABMIL	LF	0.558 \pm 0.082	0.571 \pm 0.063	0.677 \pm 0.054
	DF	0.622 \pm 0.063	0.561 \pm 0.054	0.691 \pm 0.069

can be complex. Some cases exhibit performance variations depending on the fusion stage emphasis, complicating model configuration and interoperability. Last, our late fusion block, incorporating MOAB, operates on latent space vectors derived from the early fusion stage, where omics features have already been blended. Consequently, pinpointing the specific CpG feature that most significantly impacts the outcome becomes challenging.

V. DISCUSSION

In CNS tumor subtyping, the integration of DNA methylation profiling with WSI data remains relatively underexplored despite its pivotal role in brain tumor diagnosis. This integration holds significant potential to address key challenges, such as differentiating fine-grained CNS tumor subtypes with

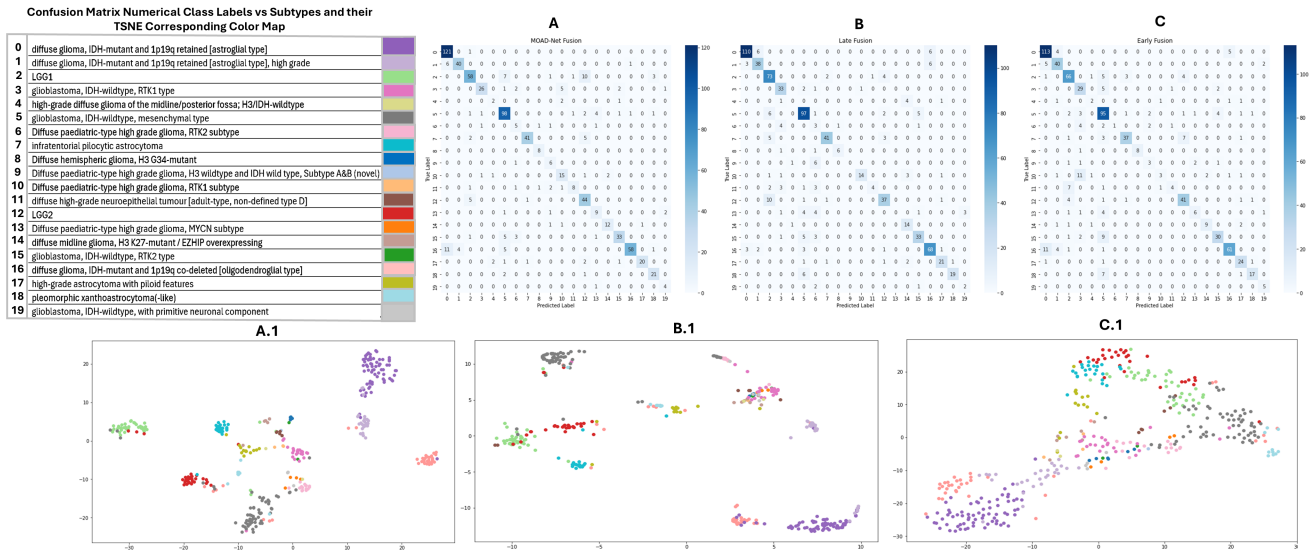


Fig. 4. Comparison of confusion matrices and t-SNE visualizations for three fusion strategies: (A) MOAD-Net, (B) Late Fusion, and (C) Early Fusion for brain tumor subtyping. The corresponding t-SNE plots are labeled as (A.1), (B.1), and (C.1), respectively.

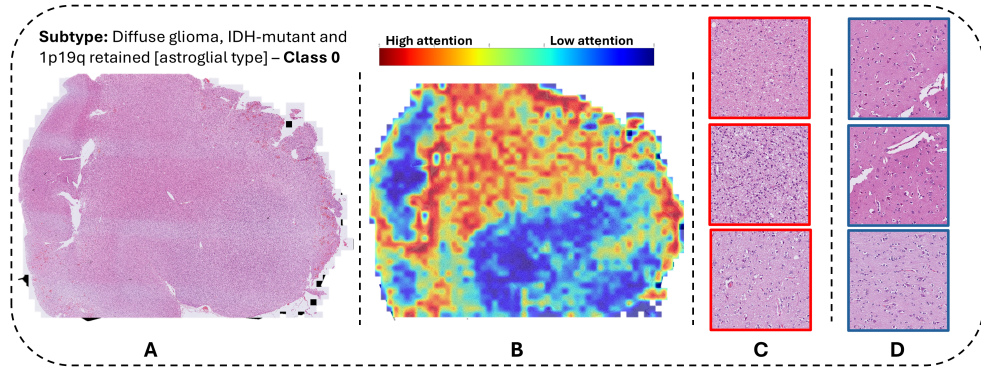


Fig. 5. Visual representation of attention heatmap generated by MOAD-Net for a diffuse glioma, IDH-mutant and 1p19q-retained (astroglial type) tumor (Class 0). (A) The original histology slide is displayed. (B) The heatmap shows areas of high attention (red) and low attention (blue), with regions of diagnostic relevance highlighted. (C) Representative patches with high attention are bordered in red, potentially indicating hallmark features of astroglial differentiation and cellular atypia crucial for diagnosis. (D) Representative patches with low attention are bordered in blue, reflecting regions of reactive gliosis or low tumor infiltration. The color bar illustrates the attention scale from high (red) to low (blue).

overlapping morphological features and managing large-scale, heterogeneous datasets. To tackle these issues, our innovative framework, MOAD-Net, incorporates DNA methylation data at multiple stages, enabling a comprehensive fusion approach. To achieve this, we propose using an MLP to map WSI patch features with DNA methylation features. This introduces nonlinearity, allowing the model to learn complex relationships while maintaining a low-dimensional representation, thus avoiding unnecessary complexity. However, we observe that when applying MOAD-Net with complex fusion models like SurvPath and MCAT, performance declines, and training becomes prolonged without effective learning. In contrast, using dual fusion embeddings $p_{i,j}$ as input to these models improves performance without introducing additional complexity. In addition to the extensive ablation studies presented in Table I, we evaluated MOAD-Net by isolating two components—early fusion and late fusion—using projected feature embeddings, $p_{i,j}$, as input to the ABMIL model. This analysis highlights the role of early fusion in enhancing overall performance and

generating interpretable heatmaps. For example, as shown in Fig. 5, the red regions of the heatmap represent a specific subtype (class 0), while the blue patches identify tumor regions that lack the defining characteristics of class 0. This demonstrates the effectiveness of post-fusion embeddings in ABMIL, which successfully separates tumor patches associated with the specific subtype, improving interpretability and performance. MOAD-Net’s use of outer arithmetic operations enables the model to capture diverse relationships between modalities, extending beyond mere additive effects. This enhanced representation is especially beneficial for tasks requiring fine-grained predictions like the complex brain tumor subtyping, as seen in the consistent improvement across all metrics in Table I. Our proposed approach also appears to scale well across different architectures, as indicated by the strong performance of models such as ACMIL and TransMIL when combined with MOAD-Net.

VI. CONCLUSION

In conclusion, the MOAD-Net framework demonstrates superior accuracy and robustness across evaluation metrics, outperforming other methods in both subtyping and survival prediction tasks. This performance highlights the unique advantages of its dual fusion strategy, combining early and late fusion to maximize predictive power and interoperability. Early fusion, by integrating omics and WSI data at the initial stages, enhances interpretability and improves classification performance through the use of ABMIL, which effectively assigns attention to crucial regions. Late fusion intermingling enriches the model's overall representation, allowing MOAD-Net to capture more complex relationships between modalities, ultimately enhancing performance across all metrics. The outer arithmetic operations—addition, subtraction, multiplication, and division—further strengthen this dual fusion approach, enabling MOAD-Net to produce a richer, more informative representation. As a result, ABMIL-MOAD-Net excels in both accuracy and consistency, making it well-suited for complex multimodal predictive tasks in precision oncology.

REFERENCES

- [1] A. Lopomo and F. Coppèdè, "Epigenetic signatures in the diagnosis and prognosis of cancer," in *Epigenetic Mechanisms in Cancer*. Elsevier, 2018, pp. 313–343.
- [2] A. Tramacere and J. Bickle, "Neuro epigenetics in philosophical focus: A critical analysis of the philosophy of mechanisms," *Biological Theory*, vol. 19, no. 1, pp. 56–71, 2024.
- [3] W.-W. Liang, R. J.-H. Lu, R. G. Jayasinghe, S. M. Foltz, E. Porta-Pardo, Y. Geffen, M. C. Wendl, R. Lazcano, I. Kolodziejczak, Y. Song *et al.*, "Integrative multi-omic cancer profiling reveals dna methylation patterns associated with therapeutic vulnerability and cell-of-origin," *Cancer cell*, vol. 41, no. 9, pp. 1567–1585, 2023.
- [4] R. Drexler, F. Brembach, J. Sauvigny, F. L. Ricklefs, A. Eckhardt, H. Bode, J. Gempt, K. Lamszus, M. Westphal, U. Schüller *et al.*, "Unclassifiable cns tumors in dna methylation-based classification: clinical challenges and prognostic impact," *Acta Neuropathologica Communications*, vol. 12, no. 1, p. 9, 2024.
- [5] L. Djirackor, S. Halldorsson, P. Niehusmann, H. Leske, D. Capper, L. P. Kuschel, J. Pahnke, B. J. Due-Tønnessen, I. A. Langmoen, C. J. Sandberg *et al.*, "Intraoperative dna methylation classification of brain tumors impacts neurosurgical strategy," *Neuro-Oncology Advances*, vol. 3, no. 1, p. vdab149, 2021.
- [6] J. C. Pickles, A. R. Fairchild, T. J. Stone, L. Brownlee, A. Merve, S. A. Yasin, A. Avery, S. W. Ahmed, O. Ogunbiyi, J. G. Zapata *et al.*, "Dna methylation-based profiling for paediatric cns tumour diagnosis and treatment: a population-based study," *The lancet child & adolescent health*, vol. 4, no. 2, pp. 121–130, 2020.
- [7] H. L. Smith, N. Wadhvani, and C. Horbinski, "Major features of the 2021 who classification of cns tumors," *Neurotherapeutics*, vol. 19, no. 6, pp. 1691–1704, 2022.
- [8] R. J. Chen, M. Y. Lu, D. F. Williamson, T. Y. Chen, J. Lipkova, Z. Noor, M. Shaban, M. Shady, M. Williams, B. Joo *et al.*, "Pan-cancer integrative histology-genomic analysis via multimodal deep learning," *Cancer Cell*, vol. 40, no. 8, pp. 865–878, 2022.
- [9] D. Capper, D. T. Jones, M. Sill, V. Hovestadt, D. Schrimpf, D. Sturm, C. Koelsche, F. Sahn, L. Chavez, D. E. Reuss *et al.*, "Dna methylation-based classification of central nervous system tumours," *Nature*, vol. 555, no. 7697, pp. 469–474, 2018.
- [10] R. J. Chen, M. Y. Lu, W.-H. Weng, T. Y. Chen, D. F. Williamson, T. Manz, M. Shady, and F. Mahmood, "Multimodal co-attention transformer for survival prediction in gigapixel whole slide images," in *Proceedings of the IEEE/CVF ICCV*, 2021, pp. 4015–4025.
- [11] R. J. Chen, T. Ding, M. Y. Lu, D. F. Williamson, G. Jaume, A. H. Song, B. Chen, A. Zhang, D. Shao, M. Shaban *et al.*, "Towards a general-purpose foundation model for computational pathology," *Nature Medicine*, vol. 30, no. 3, pp. 850–862, 2024.
- [12] D.-T. Hoang, E. D. Shulman, R. Turakulov, Z. Abdullaev, O. Singh, E. M. Campagnolo, H. Lachungnunga, E. A. Stone, M. P. Nasrallah, E. Ruppin *et al.*, "Prediction of dna methylation-based tumor types from histopathology in central nervous system tumors with deep learning," *Nature Medicine*, pp. 1–10, 2024.
- [13] G. Jaume, A. Vaidya, R. J. Chen, D. F. Williamson, P. P. Liang, and F. Mahmood, "Modeling dense multimodal interactions between biological pathways and histology for survival prediction," in *Proceedings of the IEEE/CVF Conference on CVPR*, 2024, pp. 11 579–11 590.
- [14] D. Capper, D. Stichel, F. Sahn, D. T. Jones, D. Schrimpf, M. Sill, S. Schmid, V. Hovestadt, D. E. Reuss, C. Koelsche *et al.*, "Practical implementation of dna methylation and copy-number-based cns tumor diagnostics: the heidelberg experience," *Acta neuropathologica*, vol. 136, pp. 181–210, 2018.
- [15] J. Hwang, Y. Lee, S.-K. Yoo, and J.-I. Kim, "Image-based deep learning model using dna methylation data predicts the origin of cancer of unknown primary," *Neoplasia*, vol. 55, p. 101021, 2024.
- [16] H. Zheng, A. Momeni, P.-L. Cedoz, H. Vogel, and O. Gevaert, "Whole slide images reflect dna methylation patterns of human tumors," *NPJ genomic medicine*, vol. 5, no. 1, p. 11, 2020.
- [17] D. Sturm, D. Capper, F. Andreiulo, M. Gessi, C. Kölsche, A. Reinhardt, P. Sievers, A. K. Wefers, A. Ebrahimi, A. K. Suwala *et al.*, "Multiomic neuropathology improves diagnostic accuracy in pediatric neuro-oncology," *Nature medicine*, vol. 29, no. 4, pp. 917–926, 2023.
- [18] P. Mobadersany, S. Yousefi, M. Amgad, D. A. Gutman, J. S. Barnholtz-Sloan, J. E. Velázquez Vega, D. J. Brat, and L. A. Cooper, "Predicting cancer outcomes from histology and genomics using convolutional networks," *Proceedings of the National Academy of Sciences*, vol. 115, no. 13, pp. E2970–E2979, 2018.
- [19] Z. Zhang, W. Yin, S. Wang, X. Zheng, and S. Dong, "Mbfusion: Multimodal balanced fusion and multi-task learning for cancer diagnosis and prognosis," *Computers in Biology and Medicine*, vol. 181, p. 109042, 2024.
- [20] Y. Zhang, Y. Xu, J. Chen, F. Xie, and H. Chen, "Prototypical information bottlenecking and disentangling for multimodal cancer survival prediction," *ICLR*, 2024.
- [21] O. Ogunidipe, Z. Kurt, and W. L. Woo, "Deep neural networks integrating genomics and histopathological images for predicting stages and survival time-to-event in colon cancer," *Plos one*, vol. 19, no. 9, p. e0305268, 2024.
- [22] A. H. Song, R. J. Chen, G. Jaume, A. J. Vaidya, A. S. Baras, and F. Mahmood, "Multimodal prototyping for cancer survival prediction," *ICML*, 2024.
- [23] Y. Zhang, H. Li, Y. Sun, S. Zheng, C. Zhu, and L. Yang, "Attention-challenging multiple instance learning for whole slide image classification," *ECCV*, 2024.
- [24] V. Ramanathan, P. Pati, M. McNeil, and A. L. Martel, "Ensemble of prior-guided expert graph models for survival prediction in digital pathology," in *International Conference on MICCAI*. Springer, 2024, pp. 262–272.
- [25] H. Liu, Y. Shi, Y. Xu, A. Li, and M. Wang, "Agnostic-specific modality learning for cancer survival prediction from multiple data," *IEEE Journal of Biomedical and Health Informatics*, 2024.
- [26] Y. Xu and H. Chen, "Multimodal optimal transport-based co-attention transformer with global structure consistency for survival prediction," in *Proceedings of the IEEE/CVF ICCV*, 2023, pp. 21 241–21 251.
- [27] A. H. Song, R. J. Chen, T. Ding, D. F. Williamson, G. Jaume, and F. Mahmood, "Morphological prototyping for unsupervised slide representation learning in computational pathology," in *Proceedings of the IEEE/CVF Conference on CVPR*, 2024, pp. 11 566–11 578.
- [28] O. Alwazzan, A. Khan, I. Patras, and G. Slabaugh, "Moab: Multi-modal outer arithmetic block for fusion of histopathological images and genetic data for brain tumor grading," in *2023 IEEE 20th ISBI*. IEEE, 2023, pp. 1–5.
- [29] J. A. Nicoll, T. Bloom, A. Clarke, D. Boche, and D. Hilton, "Brain uk: Accessing nhs tissue archives for neuroscience research," *Neuropathology and Applied Neurobiology*, vol. 48, no. 2, p. e12766, 2022.
- [30] J. I. Orozco, T. A. Knijnenburg, A. O. Manughian-Peter, M. P. Salomon, G. Barkhoudarian, J. R. Jalas, J. S. Wilmott, P. Hothi, X. Wang, Y. Takasumi *et al.*, "Epigenetic profiling for the molecular classification of metastatic brain tumors," *Nature communications*, vol. 9, no. 1, p. 4627, 2018.
- [31] Z. Shao, H. Bian, Y. Chen, Y. Wang, J. Zhang, X. Ji *et al.*, "Transmil: Transformer based correlated multiple instance learning for whole slide image classification," *Advances in Neural Information Processing systems*, vol. 34, pp. 2136–2147, 2021.

- [32] G. Klambauer, T. Unterthiner, A. Mayr, and S. Hochreiter, “Self-normalizing neural networks,” *Advances in NeurIPS*, vol. 30, 2017.
- [33] M. Ilse, J. Tomczak, and M. Welling, “Attention-based deep multiple instance learning,” in *ICML*. PMLR, 2018, pp. 2127–2136.
- [34] G. Jaume, L. Oldenburg, A. Vaidya, R. J. Chen, D. F. Williamson, T. Peeters, A. H. Song, and F. Mahmood, “Transcriptomics-guided slide representation learning in computational pathology,” in *Proceedings of the IEEE/CVF Conference on CVPR*, 2024, pp. 9632–9644.
- [35] Z. Liu, H. Mao, C.-Y. Wu, C. Feichtenhofer, T. Darrell, and S. Xie, “A convnet for the 2020s,” in *Proceedings of the IEEE/CVF Conference on CVPR*, 2022, pp. 11 976–11 986.
- [36] C. Xiong, H. Chen, H. Zheng, D. Wei, Y. Zheng, J. J. Sung, and I. King, “Mome: Mixture of multimodal experts for cancer survival prediction,” in *International Conference on MICCAI*. Springer, 2024, pp. 318–328.
- [37] L. Long, J. Cui, P. Zeng, Y. Li, Y. Liu, and Y. Wang, “Mugi: Multi-granularity interactions of heterogeneous biomedical data for survival prediction,” in *International Conference on MICCAI*. Springer, 2024, pp. 490–500.